Linewidths of photoinduced L x rays of uranium

J. Hoszowska, J.-Cl. Dousse, and Ch. Rhême
Physics Department, University of Fribourg, CH-1700 Fribourg, Switzerland
(Received 28 January 1994)

High-resolution measurements of the photoinduced L x-ray spectrum of metallic uranium were performed with a transmission-type bent-crystal spectrometer. Linewidths of 32 L x-ray emission lines were extracted. Nonlifetime broadening effects, such as multiple-vacancy configuration states and multiplet splitting, that influence the line profiles are discussed.

PACS number(s): 32.30.Rj, 32.70.Fw, 32.70.Jz

I. INTRODUCTION

We report on high-resolution measurements of the widths of photoinduced emission lines in the L x-ray spectrum of uranium. Vacancy lifetimes are of interest and value in several respects. They are important in studies of fluorescence yields and line shapes and provide a sensitive test of theoretical models. Accurate data for the L shell are particularly scarce for high-Z elements and discrepancies exist between the theoretical and experimental linewidths.

The natural width of an x-ray line represents the sum of the widths of the initial and final atomic states of the transition. The width of an atomic state containing an inner-shell vacancy is related to the mean lifetime of the hole by Heisenberg uncertainty relation $\Gamma\tau=\hbar$. This finite lifetime gives a Lorentzian contribution to the x-ray spectral line:

$$I(E)=I(E_0)\frac{\left[\frac{\Gamma(A)+\Gamma(B)}{2}\right]^2}{(E-E_0)^2+\left[\frac{\Gamma(A)+\Gamma(B)}{2}\right]^2}, \quad (1)$$

where $I(E)$ is the intensity at energy E, E_0 is the center of the Lorentzian, and $\Gamma(A)$ and $\Gamma(B)$ are the total natural widths of the initial and final states, respectively. The total natural width of a level $\Gamma(i)$ is the sum of the radiative $\Gamma_R(i)$, Auger $\Gamma_A(i)$, and Coster-Kronig $\Gamma_{CK}(i)$ widths.

Information on natural widths can be derived from measurements of x-ray emission lines, absorption edges, and photoelectron and Auger line shapes. However, the natural width of a state that is governed solely by the time the system occupies that state cannot be observed experimentally, being influenced by various broadening effects. The same holds for transitions between atomic levels. The broadening due to a finite instrumental response can be accounted for by convolution or deconvolution with the measured instrumental resolution function. Other contributions to the broadening stemming from shake and Coster-Kronig-Auger processes, exchange interaction, and solid-state effects being difficult to evaluate, complicate the extraction of the natural width or linewidth from the experimental profiles. It is evident that the origin and magnitude of the broadening in the experimentally observed linewidths depend on whether the levels under investigation are deep core levels or shallow ones. The effect of multiple vacancy configurations can only be negligible provided the additional holes are present in the outermost levels. Otherwise, the occurrence of multiple vacancies can affect the level widths. The change in the peripheral electron configuration of the atom in a solid could result in a change of level energies and Coster-Kronig decay channels may either open or close. Of importance is also the interaction of core levels of an atom in its metallic state with the crystal lattice environment. A review of the broadening contributions can be found in [1,2].

The paper is organized as follows. Section II deals with the experimental procedure and the method of analysis. In Sec. III the results will be presented and the effects responsible for broadening of the U L x-ray emission lines will be discussed. The summary and concluding remarks are given in Sec. IV.

II. EXPERIMENT AND DATA TREATMENT

The measurements of the x-ray spectra were carried out at the University of Fribourg, with a high-resolution transmission-type bent-crystal spectrometer. A detailed description of a similar spectrometer which is installed at the Paul Scherrer Institute, Villigen, Switzerland can be found in [3].

The spectrometer was equipped with a 1-mm-thick quartz crystal, bent to a radius of curvature of 3.13 m. The (110) reflecting planes were used for diffraction of x rays, and the reflecting area was 55×48 mm^2. The angular range of the spectrometer is $\pm20°$. For the (110) reflecting planes of a quartz crystal it corresponds theoretically to a minimum photon energy of about 7.5 keV in first order. The reflection angles were measured with an optical laser interferometer. Its accuracy varied between 3 and 5 marcsec throughout the angular range (6.7°–12.5°) corresponding to the observed L x-ray spectrum of U.

A 25-mm-high and 4-mm-wide self-supported metallic target of uranium, 48 mg/cm^2 thick, was used. The target was kept stretched by a spring in a special holder as shown in Fig. 1(a). L emission was induced by means of an Au anode x-ray tube operated at 80 kV and 35 mA.

The distance between the x-ray tube and the target was 45 mm and the tube was oriented so that the ionizing radiation was emitted perpendicularly to the target-crystal direction [Fig. 1(b)]. In preliminary measurements thinner 25.2-mg/cm^2 targets were also employed. However, when exposed for a long time to the x-ray tube radiation they deteriorated substantially. During these measurements a weak but not negligible contamination of the uranium spectrum was observed due to a coherent scattering by the target of a number of characteristic Au L x-ray lines from the tube anode. For that reason the L_3-M_1, L_3-M_4, and L_3-M_5 lines of U were measured with a 250-mg/cm^2-thick aluminum absorber placed between the tube and the target.

The spectrometer was operated in modified DuMond slit geometry. In this geometry, represented schematically in Fig. 2, a slit 0.15 mm wide located on the focal circle at a fixed position served as the effective source of radiation. The slit consisted of two 2-mm-thick juxtaposed pieces of lead. The target was placed 21 mm behind the slit and tilted at 10° to the target-crystal direction. This angle represents a compromise between two effects influencing the intensity of the observed x rays: the self-absorption of the emitted x rays in the target and the part

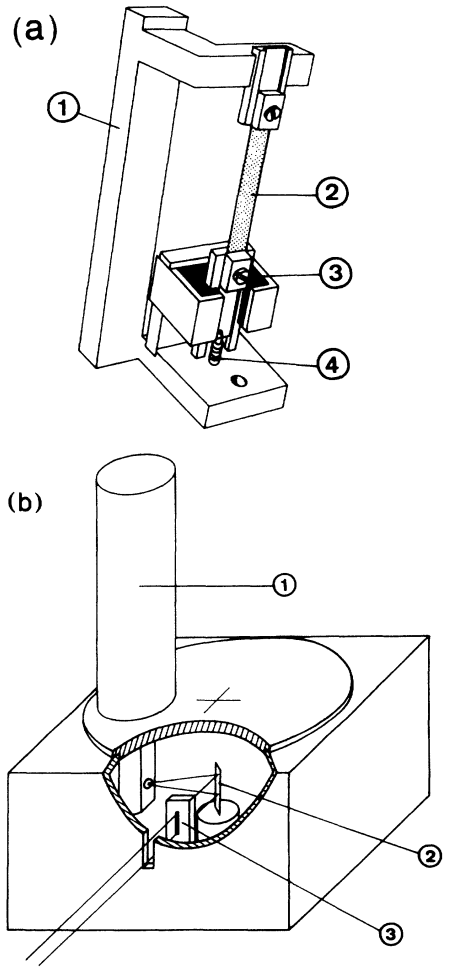

FIG. 1. (a) Target holder: (1) aluminium frame, (2) target, (3) graphite, and (4) spring. (b) Target chamber: (1) x-ray tube, (2) arget, and (3) slit.

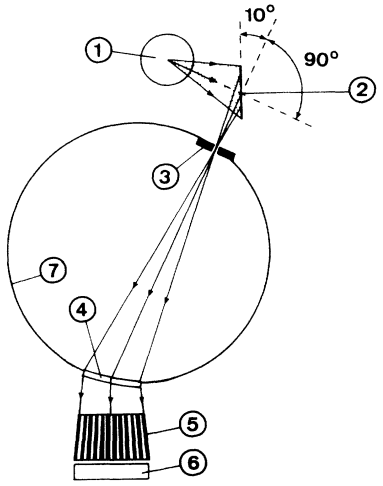

FIG. 2. Schematic diagram of the modified DuMond slit geometry (not to scale): (1) x-ray tube, (2) target, (3) slit, (4) crystal, (5) Soller slit collimator, (6) scintillation detector, and (7) focal circle.

of the target seen by the crystal through the slit. The conventional narrow source DuMond geometry (target aligned in the direction of observation, no slit) is less appropriate for measuring low-energy photons, the self-absorption being much stronger. In addition, in the slit geometry the observed line shapes are not affected by thermal deformation of the target.

In order to reduce the absorption of x rays in air, evacuated tubes were installed between the target and the crystal as well as between the crystal and the Soller slit collimator. The latter consisting of 24 parallel slits 660 mm long, 110 mm high, and 2 mm wide was also kept at a low air pressure. Regarding the absorption of x rays the crystal thickness is of prime importance. Thanks to a new bending device, similar in its principle to the system described in Ref. [4], we were able to bend properly a 100×100 mm^2 quartz crystal having a thickness of only 1 mm. As a result of these improvements, x rays with energies down to 11.6 keV (L_3-M_1 transition) could be observed with good peak-to-background conditions (see, for instance, Fig. 7). We emphasize this point because the photon energy region comprised between 10 and 20 keV is rather unfavorable for crystal diffractometry measurements. Transmission-type crystal spectrometers are operated mostly above 20 keV, while reflection-type ones are generally used below 10 keV. The lack of accurate experimental data concerning L x rays of heavy elements certainly results from that instrumental difficulty.

The x rays were recorded with a 5-in.-diam Phoswich scintillation detector. Phoswich is a trademark[1] for a two-component detector which consists of a front thin NaI crystal optically coupled to a rear thick CsI crystal. Both crystals are mounted on the same photomultiplier tube. Their signals have different rise times and can be identified by pulse shape analysis. Compton events in the

[1]The Harshaw Chemical Co., Crystal and Electronic Products Dept., OH 94139.

front scintillator producing a signal in the rear one can thus be discriminated. The Phoswich detector used in our experiment was equipped with a 0.25-in.-thick NaI crystal and a 2-in.-thick CsI crystal. Its full width at half maximum (FWHM) resolution was about 4 keV at 20 keV. Owing to the above-mentioned detector characteristics and a heavy lead shielding, a very low background was achieved. The measured natural background had, for instance, a value of 0.002 counts $\text{keV}^{-1}\,\text{sec}^{-1}$ at 20 keV. With the x-ray tube on (80 kV, 35 mA), the background arising mainly from the x-ray tube bremsstrahlung, which was scattered coherently by the target and partly diffracted by the crystal into the detector, increased by a factor of about 10.

The instrumental response was determined by measuring the 63.120 81-keV γ-ray line from the ^{169}Yb decay [5]. As the angular resolution stemming mainly from the width of the slit, the crystal mosaicity, and curvature depends slightly on the Bragg angle, the γ-ray line was recorded in the third, fourth, and fifth order of reflection, i.e., at angles in the angular range of interest. For illustration, the line profile measured in third order and approximated by a Gaussian is shown in Fig. 3. The FWHM corresponds to about 11.5 arcsec of angular resolution. The best angular resolution is obtained when the slit-to-crystal distance is adjusted for each x-ray line. However, when the x-ray spectrum extends over a large angular range and comprises many weak lines this optimization is not so convenient. It is more practical to measure a selected group of lines with an average value of the focusing distance. In consequence, only a slightly worse instrumental resolution results. Having measured the instrumental line profile for different values of the focusing distance, we were able to take this into account. The functional dependence is shown in Fig. 4. The energy widths Γ_E can be deduced from the angular widths Γ_θ from the following relation:

$$\Gamma_E = E\cot(\theta)\Gamma_\theta\,, \tag{2}$$

where E and θ are the energy and Bragg angle, respectively, of the observed lines. For the energy calibration of the spectrum, the lattice spacing constant of the (110) reflecting planes and the angular position of the zero Bragg angle are needed. The spacing constant was deduced from the above-mentioned ^{169}Yb measurements, giving a value of 2.456 553(3) Å. The zero Bragg angle may change when varying the focusing distance. For that reason, it was determined for each group of lines observed at the same focusing distance, by measuring the most intense line of the group at positive and negative Bragg angles.

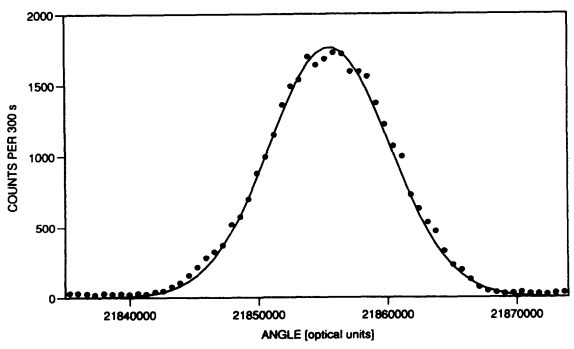

FIG. 3. The experimental response function observed with the 63.120 81-keV γ-ray line from ^{169}Yb decay measured in the third order of reflection.

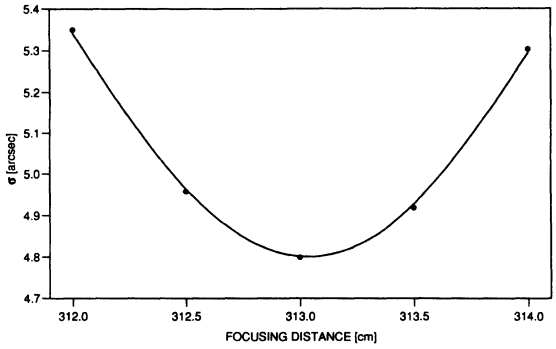

FIG. 4. The instrumental broadening versus the focusing distance (σ is the standard deviation of the Gaussian response). The measurements were performed with the 63.120 81-keV γ-ray line in the third order of reflection.

The observed spectral lines were analyzed by means of a least-squares-fitting program employing Voigt functions. The Voigt profile results from the convolution of a Lorentzian representing the natural x-ray line shape with a Gaussian. The widths of the x-ray lines were extracted by keeping fixed in the fit the known Gaussian experimental broadening.

III. RESULTS AND DISCUSSION

The measured values of the linewidths and energies of 32 L x-ray transitions of U are listed in Tables I and II, respectively. The errors quoted are statistical errors obtained from the error matrix of the least-squares-fit program. Our experimental values are compared with other available data and with theoretical predictions.

In the current work we will focus on the linewidths of the emission lines. Nonlifetime broadening effects pertinent to the widths of the presently investigated U lines will be discussed. The observed satellite structures will be analyzed in terms of their influence on the linewidths. Special attention will also be given to the broadening of the outer levels and the energy splitting of the L_1-O_3, L_3-O_1, and L_2-O_1 transitions.

A. Effect of multiple-vacancy configurations on the experimental L x-ray linewidths

Upon examining the values of the reported linewidths, it can be seen that the expected general trend $\Gamma_{L_1Y_k} > \Gamma_{L_2Y_k} > \Gamma_{L_3Y_k}$ attributed to the decrease in Coster-Kronig-Auger decay with increasing angular momentum is satisfied. However, one might be astounded by an apparent inconsistency when comparing widths of a number of transitions from the same level but leading to the different L subshells. The differences $\Gamma_{L_iY_k}$-$\Gamma_{L_jY_k}$ do not fall to common values within the experimental un-

certainties, which would have been the case if all the widths of the observed x-ray lines were virtually identical with the natural ones.

A clue to the finding is given by the observed resolved nondiagram x rays accompanying transitions to the L_3 state and not noticeable for the transitions to the L_1 and L_2 subshells. They are associated with states of multiple-vacancy configurations. In inner-shell photoionization multiple excitation or ionization may be induced by processes of the Coster-Kronig-Auger type and also by shakeup and shakeoff, while direct multiple ionization is considered to be negligible.

The Coster-Kronig (CK) transition refers to a nonradiative process of the type X_i-$X_j Y_k$, where X_i and X_j pertain to the same shell. Hence, for L-shell ionization it transfers initial L_1 vacancies to L_2 and L_3 subshells, the L_2 vacancies to the L_3 subshell, and creates an additional hole predominantly in the innermost shell that can take part energetically. In effect $L_{2,3}Y_k$ double-hole states are produced.

The interaction of x rays with atoms is a relatively weak process, in a perturbation sense, in which a single photon can be assumed to interact primarily with a single electron in a given subshell. However, inner-shell photoionization may be accompanied by the excitation of a second electron to a bound state or ejection to a continuum level. This process usually called shakeup and shakeoff results from a sudden change of the central potential as viewed by the electrons [6]. Predictions for the L shakeoff probabilities for U following the sudden approximation method of [6] are reported in [7]. The calculated probabilities P_X of shakeoff in different shells X

TABLE I. The measured linewidths of photoinduced L x-ray emission lines of uranium. The experimental results of this work are compared to the data from four experiments and two theories.

	Width (eV)						
Line	This work	Expt. Ref. [30]	Expt. Ref. [32]	Expt. Ref. [33]	Expt. Ref. [34]	Calc. Ref. [35]	Calc. Ref. [36]
L_1-M_2	31.12±0.25	24.62±0.95	32.30		27.50	35.90	
L_1-M_3	23.71±0.39	22.44±1.09	18.80		23.70	33.30	
L_1-M_4	19.54±0.50						
L_1-M_5	19.06±0.36	24.75±1.63					
L_1-N_2	25.62±0.12	26.65±0.54	39.40				
L_1-N_3	24.57±0.12	24.48±1.09	32.40				
L_1-N_4	18.14±1.76						
L_1-N_5	19.33±1.00						
L_1-O_2	25.35±0.77						
L_1-O_3^{I}	22.20±1.03						
L_1-O_3^{II}	25.74±3.77						
L_1-$O_{4,5}$	19.20±3.59						
L_1-$P_{2,3}$	26.23±1.00						
L_2-M_1	25.39±0.19	18.49±0.54					
L_2-M_4	13.14±0.06	12.24±0.27	14.30	12.71	13.50	14.50	12.33
L_2-N_1	21.36±0.38	19.17±0.95					
L_2-N_3	18.89±2.97						
L_2-N_4	14.73±0.04	15.64±0.54	15.92	15.7			
L_2-N_6	10.19±0.36						
L_2-O_1^{I}	27.20±1.62						
L_2-O_1^{II}	26.98±4.87						
L_2-$O_{4,5}$	15.33±0.05	13.05±0.54	16.36				
L_3-M_1	26.97±1.30	21.21±0.82					
L_3-M_4	13.79±0.07	12.51±0.27	14.40	12.11	12.4	10.10	11.92
L_3-M_5	13.54±0.12	11.15±0.27	13.20	12.02	12.4	9.8	11.82
L_3-N_1	21.00±0.02	19.72±0.54	19.42				
L_3-N_4	12.63±0.20	13.05±0.41					
L_3-N_5[a]	16.34±0.02	11.97±0.41	16.08	13.30	13.02		
L_3-N_6	7.43±1.68						
L_3-N_7	8.73±0.52	8.29±0.54					
L_3-O_1^{I}	29.26±2.26						
L_3-O_1^{II}	23.35±1.70						
L_3-$O_{4,5}$	11.94±0.17	11.56±0.68	11.88				
L_3-P_1	12.10±2.40						
L_3-$P_{2,3}$	28.18±8.40						

[a]Measurement with the x-ray tube voltage set at 20 kV yields a value of 14.10±0.25 eV.

when a single hole is created in the L_1 subshell are $P_M=0.001$, $P_N=0.015$, $P_O=0.064$, $P_P=0.106$, and $P_Q=0.263$ and in the $L_{2,3}$ subshells $P_M=0.0012$, $P_N=0.0167$, $P_O=0.063$, $P_P=0.108$, and $P_Q=0.263$. It can be seen that, as the inner-shell electrons of heavy atoms are subjected to a strong nuclear potential, this two-electron transition induced by single-photon absorption is of importance only for the most outer-shell electrons.

The removal of the electrons by CK and shake processes reduces the screening of the nuclear charge, resulting in an increase of the binding energies of the levels. As a consequence, x-ray satellites originate with energies shifted with respect to the energy of the diagram transition. The energy shifts for satellite x rays increase with the principle quantum number of the transition electron and decrease with the principal quantum number of the spectator vacancy. Thus, for heavy elements multiple-vacancy configurations originating from LM double-hole states give rise to resolved satellites while those from the LN and LO ones are in general hidden within the parent lines. An extensive tabulation of calculated energies for

TABLE II. The measured energies of photoinduced L x-ray emission lines of uranium. The experimental results of this work are compared to the data from two experiments and one theory.

	Energy (eV)			
Line	This work	Expt. Ref. [37]	Expt. Ref. [38]	Calc. Ref. [39]
L_1-M_2	16 575.6±0.1	16 575.3	16 578.0	16 577.0
L_1-M_3	17 455.5±0.1	17 455.0	17 455.0	17 454.0
L_1-M_4	18 029.3±0.2	18 031.0	18 031.0	18 030.0
L_1-M_5	18 204.9±0.1	18 205.4	18 207.0	18 206.0
L_1-N_2	20 484.5±0.1	20 484.7	20 486.0	20 485.0
L_1-N_3	20 712.5±0.1	20 712.7	20 714.0	20 713.0
L_1-N_4	20 977.6±0.6	20 979.0	20 979.0	20 978.0
L_1-N_5	21 018.6±0.4	21 019.0	21 019.0	21 020.0
L_1-O_2	21 498.1±0.1	21 498.4	21 494.0	21 498.0
L_1-O_3^{I}	21 538.8±0.5			
L_1-O_3^{II}	21 559.7±1.7	21 562.0	21 564.0	21 563.0
L_1-O_4	21 657.7±1.4	21 657.0	21 654.0	21 655.0
L_1-O_5	21 657.7±1.4	21 657.0	21 663.0	21 662.0
L_1-P_2	21 727.3±1.7	21 729.0		21 731.0
L_1-P_3	21 727.3±1.7	21 729.0		21 741.0
L_2-M_1	15 399.3±0.1	15 399.7	15 400.0	15 400.0
L_2-M_4	17 219.5±0.2	17 220.0	17 220.0	17 220.0
L_2-N_1	19 506.9±0.1	19 507.2	19 507.0	19 506.0
L_2-N_3	19 901.3±0.8	19 907.0	19 903.0	19 903.0
L_2-N_4	20 167.3±0.1	20 167.1	20 168.0	20 168.0
L_2-N_6	20 556.8±0.2	20 556.0	20 556.0	20 556.0
L_2-O_1^{I}	20 622.2±0.7	20 621.0	20 624.0	20 624.0
L_2-O_1^{II}	20 637.6±1.1			
L_2-O_4	20 842.5±0.1	20 842.6	20 843.0	20 845.0
L_2-O_5	20 842.5±0.1	20 842.6	20 852.0	20 852.0
L_3-M_1	11 621.7±0.3	11 618.3	11 622.0	11 620.0
L_3-M_4	13 439.7±0.1	13 438.8	13 442.0	13 440.0
L_3-M_5	13 616.0±0.1	13 614.7	13 618.0	13 616.0
L_3-N_1	15 727.9±0.1	15 726.0	15 729.0	15 726.0
L_3-N_4	16 386.8±0.1	16 385.0	16 390.0	16 388.0
L_3-N_5[a]	16 430.1±0.1	16 428.3	16 430.0	16 430.0
L_3-N_6	16 774.5±1.0		16 778.0	16 776.0
L_3-N_7	16 786.2±0.3	16 785.9	16 789.0	16 788.0
L_3-O_1^{I}	16 842.4±1.8	16 845.0	16 846.0	16 844.0
L_3-O_1^{II}	16 856.9±0.9			
L_3-O_4	17 068.6±0.1	17 070.1	17 065.0	17 065.0
L_3-O_5	17 068.6±0.1	17 070.1	17 074.0	17 072.0
L_3-P_1	17 097.0±0.7	17 096.0		17 124.0
L_3-P_2	17 119.0±1.2	17 118.0		
L_3-P_3	17 119.0±1.2	17 118.0		17 151.0

[a]Measurement with the x-ray tube voltage set at 20 kV yields a value of 16 429.1±0.1 eV.

$_{92}$U L x-ray satellites that arise from electric dipole and quadrupole transitions in the presence of one spectator hole in the M or N shell can be found in [8]. We have used these theoretical energies in the analysis and identification of the observed satellites in the measured L x-ray spectrum of uranium.

For uranium according to the calculated transition rates from [9], the additional M holes due to L_1-$L_3Y_{\hat{k}}$ CK processes are predominantly created in the $M_{4,5}$ subshells. The probability for producing M_3 hole states by the L_1-L_3M_3 CK is several times smaller, and it is quite likely that the M_3 hole is subsequently transferred to the $M_{4,5}$ subshells by the M_3-$M_{4,5}N_k$ transitions. The L_1-L_2M_k and L_2-$L_3M_{1,2,3,4}$ CK processes are energetically impossible.

Since our data do not reveal any resolved satellite structure or asymmetry of the line profiles for the transitions to the L_1 level nor to the L_2 one (see, e.g., Fig. 5), it may therefore be assumed that the M-shake events are negligible which is in accordance with the theoretical P_M values.

For the N shakeoff and shakeup probability no definitive conclusion can be drawn, since as already pointed out the satellites originating from LN multiple hole states are embedded within the natural width of the diagram lines. In addition, spectator N holes can also be created by L_1-L_2N_k, L_1-L_3N_k, and L_2-L_3N_k CK transitions. However, it should be emphasized that the N additional vacancies could broaden the L x-ray emission lines.

A particularly clear example of the measured satellite spectrum can be seen on the high-energy side of the L_3-N_4 and L_3-N_5 lines represented in Fig. 6(a). The observed peak structure in the satellite spectrum is due to multiplet splitting of the initial and final double-hole states. Similarly, x-ray satellite components were observed for the L_3-N_1 transition. For the L_3-M_1 (Fig. 7), L_3-M_5 (Fig. 8), and L_3-M_4 transitions the satellite structure is less apparent and manifests itself as a marked asymmetry on the high-energy side of the line profiles.

Comparing the energies of these satellites with those from Ref. [8], one can conclude that they are due to the presence of M spectator vacancies during the time of the x-ray transition. The average energy shifts of these nondiagram transitions pertaining to the mentioned emission lines are larger than their natural broadening. However,

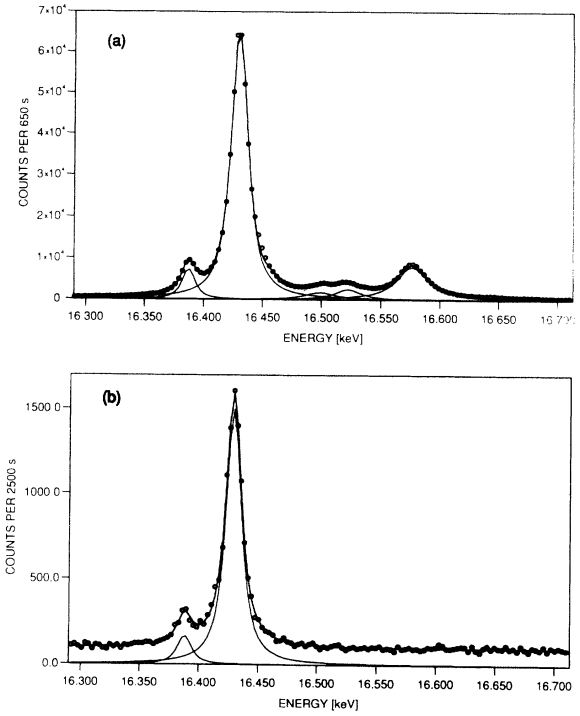

FIG. 6. The L_3-$N_{4,5}$ transitions with the accompanying M satellite structure components shifted by 72 and 89 eV with respect to the L_3-N_5 line and the L_1-M_2 transition. The L emission was induced with the x-ray tube operated at (a) 80 kV and (b) 20 kV.

satellite components that are not well separated from the emission lines lead to broadening of the linewidths. The linewidths $\Gamma_{L_3M_k}$ being larger than the $\Gamma_{L_2M_k}$ ones indicate that it is the case.

For the L_i-N_k transitions the energy shifts of the components arising from LM doubly ionized states are about twice as large as for the L_i-M_k lines and are greater the more outer the N_k final hole state is. However, the energy separation of L_3-N_4 and L_3-N_5 lines is such that the M satellites of L_3-N_4 fall on the flank of the L_3-N_5 x-ray line and thus they could increase its linewidth. Evidence to whether this is the case can be provided by observing the transitions in question with the energy of the incident

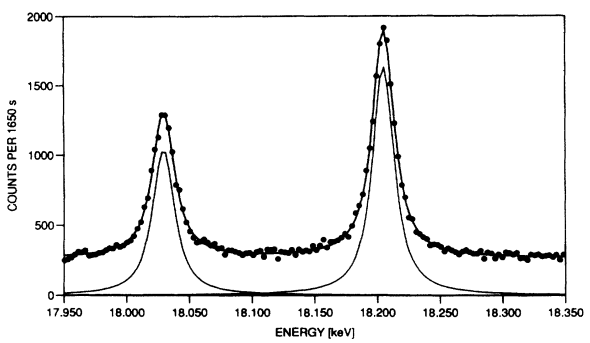

FIG. 5. The L_1-$M_{4,5}$ quadrupole doublet.

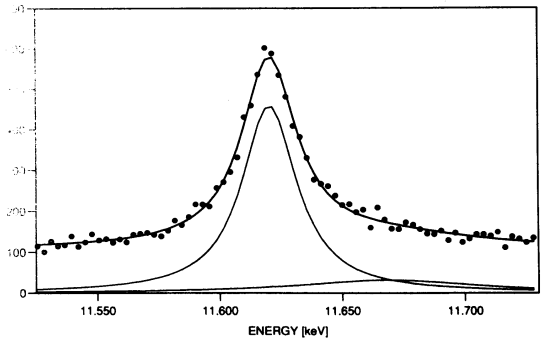

FIG. 7. The L_3-M_1 transition with M satellite structure.

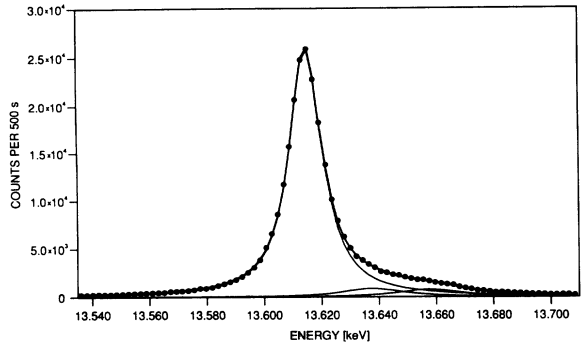

FIG. 8. The L_3-M_5 emission line with M satellites.

photons below the L_2 ionization threshold (20.948 keV). We have therefore remeasured the energy region comprising the L_3-N_4, L_3-N_5, and L_1-M_2 lines, operating the x-ray tube at 20 kV instead of 80 kV. The observed part of the x-ray spectrum is presented in Fig. 6(b). The absence of satellite structures present in the previously recorded spectrum clearly indicates that they were due to L_1-L_3M_k CK processes. The fit of the L_3-N_5 transition yields for the linewidth a value of 14.10±0.25 eV instead of 16.34±0.02 eV at 80 kV and for the energy 16429.0±0.01 eV (see Table II), confirming that M multiple hole states indeed did broaden the investigated line. The linewidth of the L_3-N_4 transition has not changed with respect to the previously extracted value, permitting us to surmise that the L_1-L_3N_k and L_2-L_3N_k CK processes do not play a significant role in broadening of the U L_i-N_k lines.

Finally, we would like to mention that a comparison with experimental results on uranium M x-ray linewidths [10] in conjunction with N level widths [11] provides valuable information on broadening of L x-ray emission lines due to multiple vacancies. The linewidths of the major M emission lines as measured by Keski-Rahkonen and Krause [10] are $\Gamma_{M_5\text{-}N_3}=15\pm2$ eV, $\Gamma_{M_5\text{-}N_6}=4.1\pm0.06$ eV, $\Gamma_{M_5\text{-}N_7}=4.1\pm0.3$ eV, $\Gamma_{M_4\text{-}N_2}=13\pm2$ eV, and $\Gamma_{M_4\text{-}N_6}=4.3\pm0.3$ eV. Adopting the natural widths $\Gamma_{M_4}=4.0\pm0.3$ eV and $\Gamma_{M_5}=3.8\pm0.3$ eV from [10], the average L_1 level width $\Gamma_{L_1}=15.4\pm0.4$ eV derived from the $\Gamma_{L_1\text{-}M_4}$ and $\Gamma_{L_1\text{-}M_5}$ linewidths (Table I) lies between the two theoretical values of 16.514 [12] and 14.0 eV [2]. Likewise, the L_2 level width $\Gamma_{L_2}=9.1\pm0.3$ obtained from the L_2-M_4 linewidth agrees with the calculated values $\Gamma_{L_1}=9.32$ [2] and 8.62 eV [12]. However, the L_3 level width, when deduced from the linewidths of the L_3-M_4 and L_3-M_5 transitions $\Gamma_{L_3}=9.8\pm0.2$ eV, is inconsistent with the theory, being larger than both estimates of 8.62 [12] and 8.204 eV [2]. Thus this comparison demonstrating the importance of the nonlifetime broadening of the transitions involving the L_3 level due to the CK processes is consistent with the earlier conclusions.

The available x-ray photoelectron spectroscopy (XPS) data on N level widths from [11] are $N_3=6.5\pm0.9$ eV, $N_4=4.0\pm0.4$ eV, and $N_5=5.5\pm1.1$ eV. Taking once again the above given values for Γ_{M_4} and Γ_{M_5}, one finds that the N_2 and N_3 level widths as derived both from M and L x-ray emission lines are consistent within the experimental uncertainties.

However, the N_3 width is large relative to the one from the XPS studies. We are inclined to explain these discrepancies by an extra broadening due to the presence of multiple vacancies during the x-ray transitions. The overlap of the resulting satellites with the diagram lines is the most plausible cause of the observed difference. For the N_4 and N_5 linewidths, we find our results to be fairly consistent with the XPS data. We would like to point out here that, contrary to McGuire's predictions [13], the calculations of Ohno and Wendin [14] predict the observed increase of the N_5 width in case of U metal where the $4d_{5/2}$-$4f5s$ CK decay channel opens (in atomic U it is closed).

B. Effect of exchange interaction on the linewidths

As a general rule we find that our experimental linewidths of the transitions from the highest occupied levels, namely O_k and P_k, are appreciably broadened and in some cases a notable splitting of emission lines is also observed. We attribute this nonlifetime broadening as due to exchange interaction between unpaired valence electrons and core holes. We also consider the possibility of a small exchange contribution to the $N_{6,7}$ widths.

The exchange interaction experiences only those core electrons which have the spin orientation as the unpaired valence electrons and it is stronger between subshells with equal principal number than with different principal quantum number. As the exchange coupling reduces the average Coulomb repulsion, the spin parallel electrons will be pulled towards the valence shell. The effect is present both in bound and free atoms. However, for an atom in the crystal field the splitting may be different from that of a free atom. In the formation of a solid, free atoms are brought close to each other and discrete energy levels broaden into bands. The partial delocalization of the valence electrons, which implies a reduced magnetic moment, leads to a poorly resolved multiplet structure. On the contrary, when the valence electrons are well localized the exchange interaction gives rise to well-defined multiplets.

The role of exchange interaction between vacancies and unfilled subshells has been demonstrated by various experiments. Multiplet splitting has been observed in photoelectron lines of $3d$ and $4d$ elements and their complexes [15,16]. In x-ray emission spectroscopy the effect of multiplet splitting on the L x-ray lines of rare earth elements has been also investigated [17,18]. For transition metals the observed asymmetry on the low-energy side of the K_α and K_β lines was suggested to be due to the exchange interaction between the electrons of the incomplete $3d$ shell and those of the unfilled inner shell owing to the emission of x rays [19]. The experimental studies of photoabsorption spectra of rare earth elements above the $4d$ edge have also demonstrated the effect of

exchange interaction on the final state $4d^9 4f^{n+1}$ configuration [20].

For actinides and their compounds, the complex line shapes of core levels and the presence of intense satellites in photoelectron spectra in XPS studies have been recognized to be related to the degree of localization of the screening orbitals. As the electronic, magnetic, and optical properties of these materials depend on the valence-band structure, numerous studies investigating the trends of localization of $5f$ electrons [21–25] have been performed. The degree of $5f$ localization depends on the overlap of the $5f$ wave functions on the neighboring atoms and on the hybridization between the $5f$ and the $6d$-$7s$ conduction band electrons. For uranium metal in the ground state the $5f$ electrons are found to be itinerant but not far from localization. Hence the magnetic properties of U lie in the regime between itinerant magnetism of the transition metals and local-moment behavior of rare earth elements [24]. According to [26,27] the valence-band structure of U consists of a narrow band that contains four electrons per atom and is derived from hybridized $5f$ or $6d$ orbitals. The two remaining electrons form a broader band derived from $7s$ orbitals hybridized with $5f$ and $6d$ ones. The band containing four electrons and associated mainly with $5f$ electrons starts about 0.3 eV below the Fermi level and has a width of about 2.5 eV [24]. The free-atom electron configuration of uranium is $5f^3 6d^1 7s^2$. In the metallic state it is found [23] that U is with equal probability tetravalent $5f^2(6d7s)^4$ or pentavalent $5f^1(6d7s)^5$. With the use of electron-energy-loss spectroscopy and XPS technique [28] it was demonstrated that in the $4f$ and $5d$ core excitation spectra of U the $5f$ screening is most effective. A comparison of the experimental results with the multiplet calculations in intermediate coupling points out that under the presence of a core hole, the $5f$ final-state wave function becomes sufficiently localized to give rise to multiplet splitting in the $5d^9 5f^{n+1}$ final state. It was also mentioned that the states could be additionally broadened by their interaction with the bulk $5f$ band and that some structure in the $5d$ spectrum could also be due to sd screening.

Likewise, we conclude that our broadened L x-ray emission lines from the highest occupied states are subject to exchange interaction splitting due to various possible multiplet states formed by coupling of a core hole produced upon L emission in a metal-atom subshell to a localized moment of the valence electrons. It should be noted, however, that in x-ray emission neither the initial nor the final state is the ground state of the atom. Configurations that involve partially filled subshells in addition to the $5f$ subshell have of course more complicated level structures [29]. Hence a simple superposition of the multiplet structure observed by means of photoelectron spectroscopy on x-ray emission lines may not be valid. The O_i and P_i level widths obtained by XPS [11] are indeed systematically smaller than ours. The theoretical total L subshell level widths are $L_1=14.0$ eV, $L_2=9.32$ eV, and $L_3=7.43$ eV from [2] and $L_1=16.514$ eV, $L_2=8.62$ eV, and $L_3=8.204$ eV from [12]. The values of the level widths determined by x-ray photoelectron spectroscopy measurements are the following: $O_2=4.5\pm1.0$ eV, $O_3=3.0\pm0.5$ eV, $O_4=0.9\pm0.3$ eV, $O_5=1.1\pm0.3$ eV, $P_1=2.3\pm0.5$ eV, $P_2=1.5\pm0.5$ eV, and $P_3=1.9\pm0.3$ eV. Thus it follows from our experimental results that the presence of a vacancy in the initial state has an appreciable influence on the structure of the multiplet components of the x-ray emission transitions. The measured N_6 and N_7 widths are 0.8 ± 0.3 eV [11] whereas the theory estimates 0.288 eV [13]. Considering the large experimental uncertainties, we find no striking difference with our values as in the case of O and P levels.

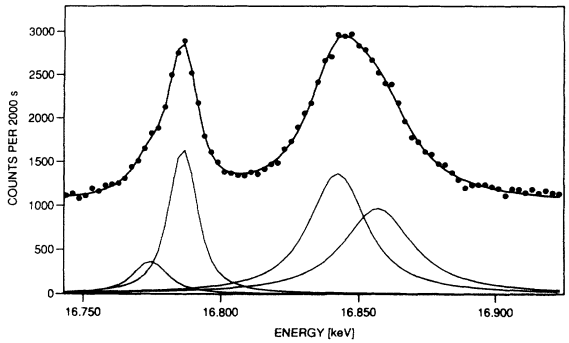

FIG. 9. The L_3-$N_{6,7}$ spin-orbit components and the L_3-O_1 transition showing a composite structure. The energies of the components are 16.842 and 16.857 keV, respectively.

The line shapes of the measured $L_{2,3}$-O_1 and L_1-O_3 transitions exhibit not only a broadening but also a composite structure. The L_3-O_1 emission line shown in Fig. 9 is distorted on the high-energy side. The fit results in two components separated by 15 eV. The splitting of the L_2-O_1 line is also about 15 eV. For the L_1-O_3 transition represented in Fig. 10 the separation of the resolved splitting components is 21 eV. It should be mentioned that splitting of this x-ray emission line has already been observed by Merrill and DuMond [30], but no suggestion about its origin was made. The $5p_{3/2}$ photoelectron spectra of U and UO_3 have shown to exhibit a smaller splitting of 5.0 and 3.2 eV, respectively [31]. The authors have suggested that it is caused by effective internal field gradients in the interior of the atom, which can be enhanced by application of a strong external electric field.

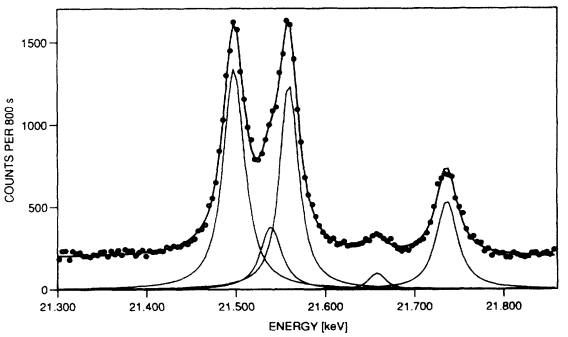

FIG. 10. The L_1-O_2 transition at 21.498 keV, the two splitting components of L_1-O_3 at 21.538 and 21.559 keV, respectively, and the L_1-$O_{4,5}$ and L_1-$P_{2,3}$ emission lines.

The splitting was considered to be due primarily to crystal-field effects regardless of the presence of the unpaired valence electrons. It should be noted that in actinides the $5f$ electrons being diffuse and not deeply buried in the core are not shielded from crystal-field interactions and are thus sensitive to the nearest-neighbor atoms. This could lead to a redistribution of the multiplet components. In this context, a study of L x-ray emission lines from the outer occupied levels of U compounds would be of interest. To our knowledge no theoretical investigation of multiplet splitting of L x-ray emission lines of U has been performed.

IV. SUMMARY AND CONCLUSIONS

In this section we would like to emphasize the most important conclusions that have emerged in the course of the investigation of the measured U L x-ray linewidths. The study performed has shown that the experimental linewidths of the transitions to the L levels of metallic uranium inferred from the photoinduced L x-ray spectrum are subject to nonlifetime broadening effects. We have demonstrated that the main contribution to the broadening of the linewidths is associated with the occurrence of multiple vacancies during the time of the x-ray transition and with exchange coupling (multiplet splitting).

The measured L_3-Y_k spectral lines were accompanied by resolved satellite structures. On the contrary, for the transitions to the L_1 and L_2 subshells no resolved nondiagram components were observed. In view of this fact, a conclusion was drawn that these nondiagram transitions arising from LM double-hole configurations are mainly due to Coster-Kronig-type processes whereas the effect of M shake events can be considered to be negligible. Satellites due to the presence of spectator vacancies in N and higher subshells coalesce with diagram lines and are not distinguishable.

It was found that the emission lines from the highest occupied states exhibit an appreciable broadening and for a number of transitions an energy splitting was also observed. This nonlifetime broadening was interpreted as due to the possible multiplet states formed by coupling of a hole in the metal-atom level to an unfilled valence subshell. In a comparison with the available XPS data, we have pointed out that the presence of the vacancy in the initial state influences the structure of the multiplet components.

Finally, for completeness we state that the agreement between experimental data from different measurements is rather poor. Also a striking discrepancy exists between the calculated and measured values of the L_1-M_2 and L_1-M_3 linewidths, indicating that the calculations overestimate the M_2 and M_3 level widths.

[1] K. D. Sevier, in *Low-Energy Electron Spectrometry* (Wiley-Interscience, New York, 1972), p. 220ff.
[2] M. Krause and J. H. Oliver, J. Phys. Ref. Data **8**, 329 (1979).
[3] B. Perny *et al.*, Nucl. Instrum. Methods A **267**, 120 (1988).
[4] W. Beer, P. F. A. Goudsmit, and L. Knecht, Nucl. Instrum. Methods A **219**, 322 (1984).
[5] E. G. Kessler, L. Jacobs, W. Schwitz, and R. D. Deslattes, Nucl. Instrum. Methods **160**, 435 (1979).
[6] T. A. Carlson and C. W. Nestor, Phys. Rev. A **6**, 2887 (1973).
[7] F. Parente, M. L. Carvasho, and L. Salgueiro, J. Phys. B **16**, 4305 (1983).
[8] F. Parente, M. H. Chen, B. Crasemann, and H. Mark, At. Data Nucl. Data Tables **26**, 383 (1981).
[9] M. H. Chen and B. Crasemann, At. Data Nucl. Data Tables **19**, 97 (1977).
[10] O. Keski-Rahkonen and M. O. Krause, Phys. Rev. A **15**, 959 (1977).
[11] J. C. Fuggle and S. F. Alvorado, Phys. Rev. A **22**, 1615 (1980).
[12] M. H. Chen, B. Crasemann, and H. Mark, Phys. Rev. A **24**, 177 (1981).
[13] E. J. McGuire, Phys. Rev. A **9**, 1840 (1974).
[14] M. Ohno and G. Wendin, Phys. Rev. A **31**, 2318 (1985).
[15] C. S. Fadley and D. A. Shirley, Phys. Rev. A **2**, 1109 (1970).
[16] R. L. Cohen *et al.*, Phys. Rev. B **5**, 1037 (1972).
[17] V. F. Demekhin, A. I. Plarkov, and M. V. Lyubivaya, Zh. Eksp. Teor. Fiz. **62**, 49 (1972) [Sov. Phys. JETP **35**, 28 (1972)].
[18] K. Tsutsumi and O. Aita, Phys. Rev. B **25**, 5415 (1982).
[19] K. Tsutsumi and H. Nakamori, J. Phys. Soc. Jpn. **25**, 1419 (1986).
[20] J. L. Dehmer, F. Starace, and U. Fano, Phys. Rev. Lett. **21**, 1521 (1971).
[21] J. C. Fuggle *et al.*, Phys. Rev. Lett. **45**, 1597 (1980).
[22] J. C. Schneider and C. Laubschat, Phys. Rev. Lett. **46**, 1023 (1981).
[23] B. Johansson, Phys. Rev. B **11**, 2740 (1974).
[24] J. F. Herbst *et al.*, Phys. Rev. B **14**, 3265 (1976).
[25] M. B. Brodsky, Rep. Prog. Phys. **41**, 1549 (1978).
[26] B. W. Vealand and D. J. Lam, Phys. Rev. B **10**, 4902 (1974).
[27] Y. Baer and J. K. Lany, Phys. Rev. B **21**, 2060 (1980).
[28] H. R. Moser *et al.*, Phys. Rev. B **29**, 2947 (1984).
[29] R. D. Cowan, *The Theory of Atomic Structure and Spectra* (University of California Press, Berkeley, 1981), p. 598.
[30] J. J. Merrill and J. W. M. DuMond, Ann. Physics (N.Y.) **14**, 166 (1961).
[31] T. Novakov and J. M. Hollander, Phys. Rev. Lett. **21**, 1133 (1968).
[32] J. H. Williams, Phys. Rev. **45**, 71 (1934).
[33] P. Amorim *et al.*, J. Phys. B **21**, 3851 (1988).
[34] S. I. Salem and P. L. Lee, At. Data Nucl. Data Tables **18**, 233 (1976).
[35] E. McGuire, Phys. Rev. A **5**, 1043 (1972).
[36] M. H. Chen, B. Crasemann, and H. Mark, Phys. Rev. A **21**, 449 (1980).
[37] J. A. Bearden, Rev. Mod. Phys. **39**, 78 (1967).
[38] E. Storm and H. I. Israel, Nucl. Data Tables **7**, 565 (1970).
[39] F. P. Larkins, At. Data Nucl. Data Tables **20**, 319 (1977).

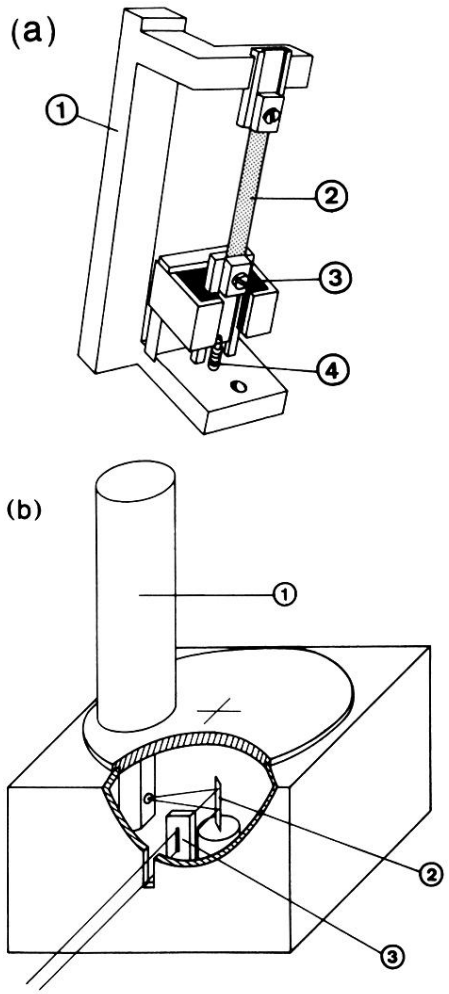

FIG. 1. (a) Target holder: (1) aluminium frame, (2) target, (3) graphite, and (4) spring. (b) Target chamber: (1) x-ray tube, (2) target, and (3) slit.

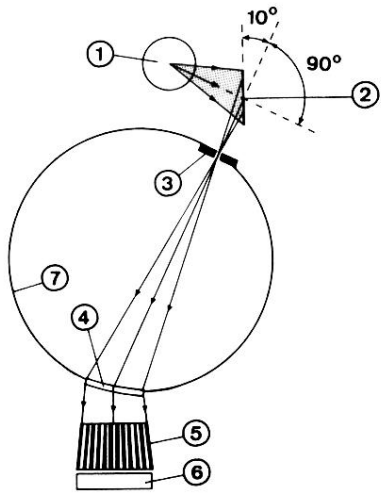

FIG. 2. Schematic diagram of the modified DuMond slit geometry (not to scale): (1) x-ray tube, (2) target, (3) slit, (4) crystal, (5) Soller slit collimator, (6) scintillation detector, and (7) focal circle.